Published in final edited form as:
Nat Genet. 2013 September ; 45(9): 995–1003. doi:10.1038/ng.2707.

DYX1C1 is required for axonemal dynein assembly and ciliary motility

Aarti Tarkar[1,*], **Niki T. Loges**[2,*], **Christopher E. Slagle**[3,*], **Richard Francis**[4], **Gerard W. Dougherty**[2], **Joel V. Tamayo**[3], **Brett Shook**[1], **Marie Cantino**[1], **Daniel Schwartz**[1], **Charlotte Jahnke**[2], **Heike Olbrich**[2], **Claudius Werner**[2], **Johanna Raidt**[2], **Petra Pennekamp**[2], **Marouan Abouhamed**[2], **Rim Hjeij**[2], **Gabriele Köhler**[5], **Matthias Griese**[6], **You Li**[4], **Kristi Lemke**[4], **Nikolas Klena**[4], **Xiaoqin Liu**[4], **George Gabriel**[4], **Kimimasa Tobita**[4], **Martine Jaspers**[7], **Lucy C. Morgan**[8], **Adam J. Shapiro**[9], **Stef J.F. Letteboer**[10,11], **Dorus A. Mans**[10,11], **Johnny L. Carson**[9], **Margaret W. Leigh**[9], **Whitney E. Wolf**[12], **Serafine Chen**[3], **Jane S. Lucas**[13], **Alexandros Onoufriadis**[14], **Vincent Plagnol**[15], **Miriam Schmidts**[14], **Karsten Boldt**[16], **UK10K**[17], **Ronald Roepman**[10,11,18], **Maimoona Zariwala**[19], **Cecilia W. Lo**[4], **Hannah M. Mitchison**[14], **Michael R. Knowles**[12], **Rebecca D. Burdine**[3], **Joseph J. LoTurco**[1,+], and **Heymut Omran**[2,+]

[1]Department of Physiology and Neurobiology, University of Connecticut, Storrs, CT 06269-3156, USA [2]Department of Pediatrics, University Hospital Muenster, 48149 Muenster; Germany [3]Department of Molecular Biology, Princeton University, Princeton, NJ 08544, USA [4]Department of Developmental Biology, University of Pittsburgh School of Medicine, Pittsburgh, PA 15201 [5]Department of Pathology, University Hospital Muenster, 48149 Muenster, Germany [6]Dr. von Haunersches Children's Hospital, Ludwig Maximilian University, 80337 Munich, Germany [7]University Hospital Leuven, Campus Gasthuisberg, 3000 Leuven, Belgium [8]Department of

[+]Corresponding and lead authors: Joseph J. LoTurco; Department of Physiology and Neurobiology; University of Connecticut; Storrs, CT 06269-3156, USA; Phone: +1-860-486-3271; Joseph.LoTurco@uconn.edu, Heymut Omran; Department of Pediatrics; University Hospital Muenster; 48149, Muenster; Germany; Phone: +49-251-8347731; heymut.omran@ukmuenster.de.
[*]Shared first author contribution.
[17]A list of members appears in the Supplementary Note

URLs
ZFIN Direct Data Submission: http://zfin.org (2004); For further information about the UK10K group: http://uk10k.org.uk; Complex congenital heart disease (CCHD) database: http://www.informatics.jax.org/javawi2/servlet/WIFetch?page=alleleDetail&id=MGI:5311375

Database accession numbers
All cDNA clones were confirmed by sequence analysis and matched the following gene accession numbers: NM_130810.3 (*DYX1C1*), NM_178452.4 (*DNAAF1/LRRC50*), BC016843 (*DNAAF3/C19orf51*), NM_213607.1 (*CCDC103*), and NM_018139.2 (*DNAAF2/KTU*).

Authors Contributions J.L. and H.O. designed the study. Authors contributing to human *DYX1C1*: N.T.L., C.J., H.Ol., R.H., G.W.D., P.P., M.A., D.A.M., S.J.F.L., R.R., K.B. and J.R. performed the experiments and analysed the human data, G.K., C.W., J.R., M.G., M.J., H.O. provided clinical OP patient data; M.Z., L.C.M., A.J. S., J.L.C., M.W.L., W.E.W. and M.R.K. performed mutational analyses and provided the clinical data from UNC patients; UCL patient clinical ascertainment: J.S.L.; UCL mutation analysis: A.O., M.S., H.M.M.; deletion algorithm for UCL patients: V.P., UK's exome sequencing: UK10K. Authors contributing to mouse *Dyx1c1*: A.T., B.S., M.C., N.T.L., P.P., M.A. performed the experiments and analysed the mouse data. Authors contributing to mouse *Sharpei*: R.F., Y.L., K.L., N.K., X.L., G.G., K.T. performed the experiments and analysed the mouse data. Authors contributing to zebrafish *Dyx1c1*: C.E.S., J.V.T., S.C., R.D.B. performed the experiments and analysed the zebrafish data. Authors contributing to Y2H experiments: D.A.M., S.J.F.L., R.R.

Author information The authors have no competing interests as defined by Nature Publishing Group, or other interests that might be perceived to influence the results and/or discussion reported in this article.

Respiratory Medicine, Concord Hospital, Concord 2139, Australia [9]Department of Pediatrics, UNC School of Medicine, Chapel Hill, NC 27599, USA [10]Department of Human Genetics, Radboud University Medical Centre, Nijmegen, The Netherlands [11]Nijmegen Centre for Molecular Life Sciences, Radboud University Medical Centre, Nijmegen, The Netherlands [12]Department of Medicine, UNC School of Medicine, Chapel Hill, NC 27599, USA [13]Primary Ciliary Dyskinesia Centre, NIHR Southampton Respiratory Biomedical Research Unit, University of Southampton and University Hospital Southampton NHS Foundation Trust, Southampton, SO17 1BJ, UK [14]Molecular Medicine Unit, Institute of Child Health, University College London, London WC1N 1EH, UK [15]University College London, Genetics Institute, London, WC1E 6BT, UK [16]Institute for Ophthalmic Research, Division of Experimental Ophthalmology and Medical Proteome Center, University of Tuebingen, D-72076 Tuebingen, Germany [18]Institute for Genetic and Metabolic Disease, Radboud University Medical Centre, Nijmegen, The Netherlands [19]Department of Pathology & Laboratory Medicine, UNC School of Medicine, Chapel Hill, NC 27599, USA

SUMMARY

Dyx1c1 has been associated with dyslexia and neuronal migration in the developing neocortex. Unexpectedly, we found that deletion of *Dyx1c1* exons 2–4 in mice caused a phenotype resembling primary ciliary dyskinesia (PCD), a genetically heterogeneous disorder characterized by chronic airway disease, laterality defects, and male infertility. This phenotype was confirmed independently in mice with a $Dyx1c1^{c.T2A}$ start codon mutation recovered from an ENU mutagenesis screen. Morpholinos targeting *dyx1c1* in zebrafish also created laterality and ciliary motility defects. In humans, recessive loss-of-function *DYX1C1* mutations were identified in twelve PCD individuals. Ultrastructural and immunofluorescence analyses of *DYX1C1*-mutant motile cilia in mice and humans revealed disruptions of outer and inner dynein arms (ODA/IDA). DYX1C1 localizes to the cytoplasm of respiratory epithelial cells, its interactome is enriched for molecular chaperones, and it interacts with the cytoplasmic ODA/IDA assembly factor DNAAF2/KTU. Thus, we propose that DYX1C1 is a newly identified dynein axonemal assembly factor (DNAAF4).

Cilia, hair-like organelles projecting from the surface of nearly all polarized cell types, serve essential roles in cellular signalling and motility[1]. The basic structure of motile cilia, and the related organelle flagellum is remarkably conserved throughout evolution. In most motile cilia, a ring of nine peripheral microtubule doublets surrounds a central pair apparatus of single microtubules that connect to the nine peripheral doublets by radial spokes (9+2 structure). Motile monocilia present at the mouse node during early embryogenesis are an exception, lacking the central pair apparatus (9+0 structure). Distinct multi-protein dynein complexes attached at regular intervals to the peripheral microtubule doublets contain molecular motors that drive and regulate ciliary motility. Specifically, outer dynein arms (ODA) are responsible for beat generation, while both the inner dynein arms (IDA) and the nexin link-dynein regulatory complexes (N-DRCs) regulate ciliary and flagellar beating pattern and frequency. Identifying the proteins responsible for correct assembly of this molecular machinery is critical to understanding the causes of motile cilia-related diseases.

Primary ciliary dyskinesia (PCD) (MIM 242650), a rare genetic disorder affecting approximately 1 in 20,000 individuals, is caused by immotile or dyskinetic cilia. Loss of ciliary function in upper and lower airways causes defective mucociliary airway clearance and subsequently, chronic inflammation that regularly progresses to destructive airway disease (bronchiectasis). Organ laterality defects are also observed with approximately half of PCD patients exhibiting *situs inversus*, and more rarely *situs ambiguus*, which can associate with complex congenital heart disease[2]. Dysfunctional sperm tails (flagella) frequently cause male infertility in PCD individuals, warranting assisted reproductive technologies. Another consequence of ciliary dysfunction, particularly evident in mouse models, is hydrocephalus caused by disrupted flow of cerebrospinal fluid through the cerebral aqueduct connecting the third and fourth brain ventricles[3]. Although ciliary dysmotility is not sufficient for hydrocephalus formation in humans due to morphological differences between the mouse and human brain, the incidence of hydrocephalus, secondary to aqueduct closure, is increased in PCD individuals[3].

Genetic analyses of PCD patients have now revealed several autosomal recessive mutations in genes encoding axonemal subunits of the ODA complexes and related components[4–12]. In addition, recessive mutations in *CCDC39* (MIM 613798) and *CCDC40* (MIM 613799) have been linked to PCD with severe tubular disorganisation and defective nexin links[13,14]. Mutations in the radial spoke head genes *RSPH4A* and *RSPH9* as well as in *HYDIN* can cause intermittent or complete loss of the central apparatus microtubules[15–17]. Two X-linked PCD variants associated with syndromic cognitive dysfunction and retinal degeneration are caused by mutations in *OFD1* (MIM 311200) and *RPGR* (MIM 312610), respectively[18, 19]. Another functional class of proteins emerging from identification of PCD causing mutations are proteins involved in cytoplasmic pre-assembly of both ODA and IDA: *DNAAF2* (*KTU*, MIM 612517)[20], *DNAAF1* (*LRRC50*, MIM 613190)[21, 22], *DNAAF3* (*C19orf51*, MIM 614566)[23] and the recently identified *LRRC6* (MIM 614930)[24].

DYX1C1 (MIM 608706), dyslexia susceptibility 1 candidate 1 gene, was initially identified as a candidate dyslexia gene due to both a single balanced translocation t(2;15)(q11;q21) coincidentally segregating with dyslexia in a family[25], and subsequent single nucleotide polymorphism (SNP) association studies. Follow-up gene association studies have provided both positive[26–28] and negative[29–31] support for association with dyslexia. Molecular and cellular analyses of DYX1C1 have indicated potential functional roles with chaperonins[32,33], estrogen receptor trafficking[34], and neuronal migration[35,36], while recent proteomic and gene expression studies have suggested a possible role in cilia[37,38].

Results

Generation of *Dyx1c1* mutant mice

In order to reveal the required biological functions of Dyx1c1, we performed a forward genetic experiment by producing an allele of *Dyx1c1* in mice in which exons 2–4 were deleted (Fig. 1a). Homozygous mutant mice (*Dyx1c1*$^{\Delta/\Delta}$) expressed no detectable Dyx1c1 protein by western blot analysis of all tissues tested, including brain and lung (Fig. 1b). Mice heterozygous for the deleted allele were viable, fertile, and not noticeably different from wild-type littermates. Homozygous mutant mice were recovered after birth from

heterozygous breeding pairs at rate deviating from the expected Mendelian ratio (295:570:87, (*Dyx1c*$^{+/+}$:*Dyx1c1*$^{\Delta/+}$:*Dyx1c1*$^{\Delta/\Delta}$), Chi=128.017, p<0.0001) but were recovered at early embryonic times (gestational days E6.5–E12) at the expected Mendelian ratio (22:43:20; Chi=0.105, p=0.85) suggesting embryonic lethality of approximately 2/3 of homozygous mutants. Homozygous mutants that survived after birth developed severe hydrocephalus by postnatal (P) day 16 (Fig. 1c), and died by P21, similar to what has been described for other mouse mutants with defective motile cilia[3,39].

In addition to hydrocephaly, postnatal homozygous mutant mice displayed laterality defects with 59% of mutants (51/87) showing *situs inversus totalis*, a complete inversion of left right asymmetry (Fig. 1d), 17% (15/87) displaying *situs ambiguous* with inverted heart and lung position relative to stomach and spleen, or inverted position of stomach and spleen relative to heart and lung position, and 24% (21/87) displaying *situs solitus*, normal left-right asymmetry. Mutations that cause disruptions in left-right asymmetry in mice[40] are known to result from defective function of motile nodal monocilia, and more specifically, the loss of cilia-generated leftward flow across the node in early embryogenesis[40]. The typical phenotype for laterality mutants is a 1:1 ratio for *situs inversus totalis* and *situs solitus* indicating a randomization of L-R patterning, although the *inv* mutant mouse shows a 100% rate of defects in L-R patterning. Even if the ratio of *situs inversus* to *situs solitus* seen in surviving *Dyx1c1* mutant mice deviates significantly from what would be expected for a 1:1 ratio of *situs inversus* to situs *solitus* (51:21, Chi: 12.5, p=0.0004), this ratio was already observed in other L-R patterning mutants like the *Dnahc5* mutant mouse[41]. Consistent with a role for Dyx1c1 function in the embryonic node where L-R patterning is established in the mouse, we found by whole mount *in situ* hybridization that *Dyx1c1* expression in the early embryo (E7.5) is restricted to pit cells of the embryonic node (Fig. 1e).

In an independent mouse ENU mutagenesis screen for congenital heart defects (CHD) of the NHLBI Bench to Bassinet Program, a mutant named *Sharpei* was recovered with a *Dyx1c1* missense mutation (c.T2A) that resulted in an altered AUG start codon, and expression of an aberrant N-terminal truncated Dyx1c1 protein product of approximately 31 kDa (**Supplementary Figure 1a**). This mutant was recovered based on the finding of complex congenital heart and therefore carefully histologically phenotyped. Some mutants with apparent *situs inversus* comprising dextrocardia with inverted lung lobation and right sided stomach also had subtle visceral organ situs defects, such as discordant left sided pancreas and spleen despite right sided stomach positioning (**Supplementary Figure 1b**). *Sharpei* mutants with complex CHD died prenatally or at birth with a spectrum of complex CHD, such as transposition of the great arteries with ventricular septal defect and coronary fistula (**Supplementary Fig. 1b and Supplementary Video 1**) or double outlet right ventricle with right atrial isomerism, muscular VSD, and atrioventricular septal defects (**Supplementary Fig. 1b and Supplementary Videos 2 and 3**). All these findings resemble congenital heart defects observed in other mouse models for PCD such as *Dnahc5* mutant mice[41].

Knockdown of *dyx1c1* in Zebrafish

Recently, Chandrasekar et al. showed by knockdown of *dyx1c1* results in phenotypes characteristically associated with cilia defects such as body curvature, hydrocephalus, cystic

kidneys and situs inversus[42]. To test whether *Dyx1c1* has an evolutionarily conserved role in establishing left-right asymmetry in vertebrates, we also performed morpholino-mediated knockdown experiments in zebrafish embryos. Zebrafish *dyx1c1* is expressed in embryonic tissues that contain motile cilia[42], including Kupffer's vesicle, which is known to play an important role in establishing the left-right axis. Morpholino knockdown of zebrafish *dyx1c1* resulted in hydrocephalus, kidney cysts and body axis curvature; phenotypes consistent with ciliary dysfunction in zebrafish. Morpholino knockdown of *dyx1c1* also produced laterality defects (Fig. 2a,b) as assessed by the position of the heart (*cmlc2*), liver (*fkd2*) and pancreas (*ins*) in *dyx1c1* morphant embryos at 48 hours post-fertilization (hpf). In a wild-type zebrafish embryo, the ventricle of the heart loops towards the right and the atrium loops towards the left and the liver is positioned to the left of the midline, and the pancreas lies to the right of the midline (Fig. 2a). This wild-type pattern was observed in 36.5% of the morphants, whereas 37.9% of the morphants showed a complete reversal of the placement of the organs (Fig. 2b). A heterotaxic phenotype was seen in 25.6% of the embryos (Fig. 2b). To investigate when dyx1c1 affects early left-right patterning, the expression of the zebrafish nodal gene *southpaw* (*spaw*) was studied in a timecourse of morpholino injected embryos. The expression of zebrafish *spaw* is restricted to the left LPM during somitogenesis prior to asymmetric organ positioning at 48 hpf[43]. At the 12- to 14-somite stage, 82.8% of the control embryos had left LPM expression of *spaw* whereas all of the morphant embryos lacked any expression of *spaw*, indicating that *spaw* initiation is delayed in the absence of *dyx1c1* (Fig. 2b). The delay in *spaw* expression upon loss of ciliary motility in KV has not been reported previously but has been observed in other ciliary motility mutants that do not affect KV structure (R.D.B. unpublished). At the 16- to 18-somite and 20- to 22-somite stage, most of the control embryos (97.7% and 98.8% respectively) had *spaw* expression in the left LPM; but the morphants displayed a randomized pattern; bilateral (30% and 30.6% resp.), left-sided (20% and 29.4% resp.), right-sided (26.3% and 30.6% resp.) or absent (23.8% and 9.8% resp.) (Fig. 2b). Thus, in the zebrafish embryo, *dyx1c1* is necessary for left-sided expression of *spaw* in the left LPM which is a crucial step for normal left-right axis development. Overall our results confirm the findings from Chandrasekar et al[42]. Furthermore, we demonstrate that knockdown of *dyx1c1* affects the left-sided expression of *spaw* consistent with an important role in the left-right axis development.

Analysis of ependymal cilia

Hydrocephalus and organ laterality defects are hallmarks of mutations that cause defects in ciliary motility in mice and zebrafish[1,3]. We therefore used light and electron microscopy as well as videomicroscopy to determine whether Dyx1c1 deficiency caused loss of motile cilia formation or a loss of cilia. Cilia extending from mouse ependymal cells of the cerebral ventricles, visualized by light microscopy, appeared similar in length and distribution in *Dyx1c1*$^{\Delta/\Delta}$ and wild-type littermates (Fig. 3a). Although cilia were abundant on respiratory epithelial cells in mutants and wild-type, cilia in mutants lacked immunofluorescence signal for both the outer dynein arm heavy chain Mdnah5, and the inner dynein arm light chain, Dnali1 (Fig. 3b,c). Loss of these dyneins from motile cilia would predict a loss of motility. We used live-cell imaging to directly assess cilia-mediated fluid flow and ciliary motility on the ependymal surface in *Dyx1c1*$^{\Delta/\Delta}$ mice. Explants or slices of the lateral ventricular

surfaces were prepared from *Dyx1c1*$^{\Delta/\Delta}$ and wild-type mice at P6. Ependymal cilia in wild-type mice continued to beat vigorously in these preparations, and created a directional fluid flow across the surface that could be visualized by the displacement of a small volume of India ink pressure injected onto the ependymal surface. This flow was present in all tested wild-type mice tested (n=6; Fig. 3d **and Supplementary Video 4**) but was completely missing in tissue obtained from all *Dyx1c1*$^{\Delta/\Delta}$ mice tested (n=4; Fig. 3d **and Supplementary Video 5**). We next examined the motility of ependymal cilia in coronal brain slices of wild-type and *Dyx1c1*$^{\Delta/\Delta}$ mice by infrared-DIC videomicroscopy. Cilia at the ependymal surface in wild-type and heterozygous mice were found to beat at a frequency of approximately 9 beats/sec (n=8; 34°C; **Supplementary Video 6**), while cilia on ependymal cells from all *Dyx1c1*$^{\Delta/\Delta}$ examined (n=4) lacked ciliary beating (**Supplementary Video 7**). Videomicroscopy of tissue slice from the third brain ventricle in newborn homozygous *Sharpei* mutants also showed completely immotile cilia (n=7, **Supplementary Video 8**). Beads added to the solution above the brain slice exhibited only random motion, while in wild-type littermate controls, the beads showed ependymal cilia generated flow (**Supplementary Video 8**). Similarly, videomicroscopy of the tracheal airway epithelia in newborn homozygous *Sharpei* mutants showed completely immotile cilia, consistent with PCD, while littermate controls showed normal rapid synchronous ciliary beat (**Supplementary Video 9**). We also assessed the motility of cilia in Kupffer's vesicle in *dyx1c1* morphant zebrafish with videomicroscopy. *Dyx1c1* morphants had cilia in Kupffer's vesicles that lacked motility compared to uninjected embryos (**Supplementary Video 10 and 11**).

Analysis of *Dyx1c1* mutant respiratory cilia

To assess the ultrastructure of respiratory cilia in mutants we obtained transmission electron micrographs of tracheal cilia. As on the ependymal surface, tracheal cilia were abundant in both wild-type and *Dyx1c1*$^{\Delta/\Delta}$ cells (Fig. 3e), but unlike tracheal cilia in wild-type mice, cilia in *Dyx1c1*$^{\Delta/\Delta}$ trachea were surrounded by cellular debris and mucus (Fig. 3e). We further examined the ultrastructure of tracheal cilia in cross sections by TEM. As shown in Fig. 3f, tracheal cilia in wild-type and mutant mice had typical 9+2 microtubular structure with intact radial spokes. In contrast, and consistent with the absence of heavy and light chain dynein subunits (Fig. 3b), cilia in *Dyx1c1*$^{\Delta/\Delta}$ mice lacked both ODA and IDA structures in respiratory cilia (Fig. 3f). Thus, the phenotype of *Dyx1c1* loss of function is a severe ciliary motility defect associated with absent axonemal ODA and IDA structures.

Mutation analysis of *DYX1C1* in PCD patients with ODA/IDA defects

The apparent conservation of function of mouse and zebrafish *Dyx1c1/dyx1c1* encouraged us to search for mutations in *DYX1C1* in patients with PCD, the human disorder connected to defective ciliary motility. Because of the observed ultrastructural phenotype and severe ciliary beating defect in *Dyx1c1*$^{\Delta/\Delta}$ mice, we considered *DYX1C1* an excellent candidate gene for PCD with abnormal axonemal ODA and IDA assembly. *DYX1C1*, located on chromosome 15q21.3, comprises 10 exons (translation starts in exon 2) and encompasses 77.93 kb of genomic DNA. In one highly inbred Irish family (UCL-200), a CNV analysis of whole exome sequence data (using ExomeDepth)[44] identified a homozygous *DYX1C1*

deletion in two affected siblings (UCL-200 II:1 and II:2; **Supplementary Figure 2a,b**). This finding was confirmed by Sanger sequencing of the deletion breakpoints and was present in heterozygous state in their carrier mother (**Supplementary Figure 2c**). The 3.5 kb deletion leads to the loss of exon 7 of *DYX1C1* (Fig. 4a). Interestingly, the same 3.5 kb deletion was also identified in individuals with PCD in five American/Australian families. Five of these individuals were heterozygous for the deletion along with a mutation in the splice donor site of exon 6, stop mutations and a frame shift mutation in the other allele (UNC-158, UNC-159, UNC-1669, UNC-1839, UNC-1171, Fig. 4a **and Supplementary Fig. 3e–h**) and one individual was homozygous for the deletion (UNC-663, **Supplementary Figure 3i**). In addition we screened all *DYX1C1* exons and adjacent intronic sequences by PCR amplification and subsequent Sanger DNA sequencing in 105 PCD individuals with combined ODA and IDA defects. Mutations were identified in ten affected individuals from nine unrelated families that predicted premature termination of translation (Fig. 4a,b **and Table 1**). In all analysed families, the mutations segregated with the disease status consistent with an autosomal recessive inheritance pattern (**Supplementary Fig. 2 and 3**). In three families, recessively inherited homozygous mutations were confirmed by sequencing of other family members (F648 II1, OP-359 II1, OP-556 II1). In another family, the PCD-affected individual, OP-86 II2, was compound heterozygous for two different mutations, with each mutation tracking uniquely to one of the parents (**Supplementary Fig. 3a**). A total of 9 human *DYX1C1* mutations were therefore defined (Supplementary Table 1). Apart from the 3.5 kb deletion and a splice site mutation, the other seven detected mutations predicted premature protein termination and clustered towards the middle of the 420 amino acid sequence between amino acids 128 and 195 (Fig. 4b). Thus, remarkably, seven of the nine identified mutations predict a truncated DYX1C1 protein that would lack more than half of the protein, including the carboxyl-terminal tetratricopeptide repeat domains (TPR). The TPR domains in DYX1C1 have been shown previously to be functionally important domains required for DYX1C1 in neuronal motility, cellular localization, and interaction with molecular chaperones[33,35].

Clinical phenotype of PCD patients carrying *DYX1C1* mutations

All twelve PCD patients with recessive *DYX1C1* mutations suffer from classical symptoms of PCD, including recurrent upper and lower airway disease and bronchiectasis. Seven patients had neonatal respiratory distress syndrome. Four patients exhibited reduced fertility (Supplementary Table 1) and one male patient was treated for infertility, having three children by assisted reproduction, suggesting a probable DYX1C1 function also in sperm tails. Five of the twelve affected individuals display *situs inversus totalis* (42%), two have *situs ambiguous* (16%), one with dextrocardia and polysplenia and one with left atrial isomerism and polysplenia, and five have *situs solitus* (42%). Thus, *DYX1C1* deficiency in PCD patients causes disruption of left-right body asymmetry, similar to findings observed in mouse and zebrafish. Interestingly, no patient was diagnosed with dyslexia or with hydrocephaly. Hydrocephalus is a common phenotype in mouse mutants with immotile cilia but rare in human patients[3,39]. Two patients had a learning disability, but these can likely be attributed to other causes including microcephaly (OP-86 II2, UCL-200 II:1).

Characterization of dynein arm defects in *DYX1C1* deficient respiratory cilia

Respiratory cilia isolated from patients with biallelic *DYX1C1* mutations displayed severe ultrastructural defects (Fig. 4c–f) resembling those defects observed in mouse *Dyx1c1* mutants (Fig. 3b,c and e). Specifically, both ODA and IDA defects were present in TEM analyses in all ten assessed probands (OP-86 II2, OP-556 II1, UNC1669, UNC1839, UNC1171, UNC158, UNC159, UNC663, UCL-200 II:1 and II:2) (Fig. 4c and Supplementary Table 1). To further understand the defect on the molecular level, we performed immunofluorescence microscopy of cilia using antibodies targeting components of the axonemal ODAs, IDAs and N-DRC. Immunofluorescence analysis revealed an absence or marked reductions of proteins normally present in type-1 and type-2 ODA complexes (DNAH5, DNAH9, and DNAI2; Fig. 4d,e **and Supplementary Fig. 4–6**) as well as IDA subtype complexes (DNALI1; Fig. 4f **and Supplementary Fig. 7**). These findings are similar to cytoplasmic pre-assembly (DNAAF) defects reported in *DNAAF2* (*KTU*)[20], *DNAAF1* (*LRRC50*)[21,22], and *DNAAF3 (C19orf51)*[23] mutant ciliary axonemes. Interestingly, we found that the extent of axonemal ODA defects varied among the respiratory cells tested, and in some cases the ODA proteins DNAH5 and DNAI2 could be detected in the axonemes (**Supplementary Fig. 4 and 6**). Assembly of proximal type-1 ODA complexes (DNAH9 negative and DNAH5 positive) appeared to be better preserved than distally localized type-2 ODA complexes (DNAH5 and DNAH9 positive; **Supplementary Fig. 4–6**). To further understand the functional consequences of our observations, we performed nasal brush biopsy in patients (F-648 II1, OP-86 II2, UNC1669, UNC1839, UNC1171, UNC663, UCL-200 II:1 and II:2) and analysed respiratory cilia beating by high-speed videomicroscopy. Videomicroscopy revealed that most respiratory cells had immotile cilia (**Supplementary Video 12 and 13**); however, cilia were found to beat in some respiratory cells, albeit with reduced frequency (**Supplementary Video 14 and 15**) when compared to control cilia (**Supplementary Video 16**). These variable motility defects in *DYX1C1* mutant cells are consistent with our previous observations of variable degrees of axonemal ODA defects. Interestingly, only mutations in *DNAAF2* (*KTU*) in human patients have revealed respiratory cells with similarly variable ODA defects and associated IDA abnormalities[20].

Cellular sublocalization and interaction partners of DYX1C1

The phenotypes described above and previously reported interactions between exogenously expressed DYX1C1 protein and molecular chaperones suggested to us that DYX1C1 may function as a newly identified cytoplasmic axonemal dynein assembly factor. Consistent with this possibility, we found by immunofluorescence that Dyx1c1 protein is located in the cytoplasm of respiratory epithelia (Fig. 5a). We confirmed this finding by immunoblot by showing that similar to DNAAF2, DYX1C1 is also present in the cytoplasmic protein fraction and almost undetectable in the axonemal protein fraction of human respiratory cells. (Fig. 5b). Considering the similarities in phenotype caused by *DYX1C1* and *DNAAF2* mutations with regard to variable ODA defects, we tested for possible interactions between these proteins. Using myc- and FLAG-tagged proteins that were coexpressed in HEK293 cells, we found by co-immunoprecipitation that DYX1C1 interacted with DNAAF2/KTU (Fig. 5c), but not the cytoplasmic pre-assembly factors DNAAF1 and DNAAF3 or the PCD-

associated protein CCDC103 that localizes in both the cytoplasm and axoneme and plays a role in dynein arm attachment (**Supplementary Fig. 8**), as well as the newly identified dynein arm assembly protein LRRC6 (data not shown). Furthermore, we demonstrate that DYX1C1 and DNAAF2 interact directly by yeast two-hybrid assay (Fig. 5d). Based on these findings, we hypothesize that DYX1C1 represents a novel cytoplasmic axonemal dynein assembly factor possibly acting together with DNAAF2/KTU at an early step of cytoplasmic ODA and IDA assembly.

To categorize the molecular function of Dyx1c1 more completely in respiratory tissue we defined the protein interactome of Dyx1c1 in mouse trachea by co-immunoprecipitation and tandem mass spectroscopy (MS/MS). Input extracts for co-immunoprecipitation were prepared from trachea tissue of either wild-type or mutant mice and these appeared similar in protein composition as evaluated by coomassie staining after SDS-PAGE (**Supplementary Fig. 8a**). Following co-immunoprecipitation with anti-Dyx1c1 antibodies coomassie stained protein bands were apparent in preparations from wild-type extracts but not in mutant extracts (**Supplementary Fig. 8a**). Fourteen matched pairs of gel pieces covering the range of approximately 20 to 200 kDa, with many pieces containing mutiple bands, were cut from wild-type and mutant co-immunoprecipitations and subjected to tryptic digest and tandem mass spectrometry analysis for protein identification. In all, 702 proteins were positively identified in immunoprecipitates from wild-type trachea, while a total of 29 proteins were identified in gel slices from the mutant immunoprecipitates (Supplementary Table 2). To determine whether the identified Dyx1c1 protein interactome was enriched for particular molecular or biological functions we used DAVID to determine the presence of enriched Panther Gene Ontology terms in the Dyx1c1 interactome and proteins identified in the knockout control. Using a mouse lung proteome as a background we found several molecular functional categories enriched in the Dyx1c1 interactome and several of these were in the categories containing molecular chaperones (MF00077: Chaperone, $p<0.001$, BP00062:Protein folding, $p<0.01$, BP00072:Protein complex assembly, $p<0.05$, and MF00078:Chaperonin, $p=0.05$, Supplementary Table 3). All four of these chaperone containing categories were not significantly enriched in the protein set identified in the mutant immunoprecipitates (Supplementary Table 3). The Dyx1c1 interactome contains a total of 28 proteins in the chaperone or chaperonin category including 6 of 8 subunits in the T-compex chaperonin complex, and multiple heat shock proteins. We confirmed by co-immunoprecipitation and western blot analysis six chaperones interacting with Dyx1c1 including Cct3, Cct4, Cct5, Cct8, Hsp70 and Hsp90 (**Supplementary Fig. 8b**).

Discussion

The protein interactions we found in tracheal tissue with endogenous Dyx1c1 are in agreement with results from a recent study using neuroblastoma cell lines and exogenously expressed Dyx1c1[45]. Our results provide the first evidence that may link the T-complex of chaperones, known primarily for their role in cytoskeletal protein assembly, to the folding and assembly of axonemal dynein complexes. Interestingly, evidence for a role of Ccts in cytoplasmic assembly of protein complexes required for motile cilia has been reported for *Tetrahymena*[46]. Although the Dyx1c1 interactome defined with tandem mass spectrometry did not include any of the known DNAAF proteins absence in an MS-MS screen does not

necessarily mean absence of potential interaction and highlights to screen for potential interactors by several means.

This study is the first to show the effects of DYX1C1/Dyx1c1/dyx1c1 deficiency in human, mouse and zebrafish. The phenotypes in all species are consistent in showing a selective defect in motile cilia reflecting deficient dynein arm transport or assembly. Furthermore, since the human patients carrying mutations in *DYX1C1* showed no evidence of dyslexia, we propose that the loss-of-function of DYX1C1 may not be a highly penetrant cause of dyslexia. In conclusion, based on the pattern of cilia defects, its cellular localization, a protein interactome enriched for chaperones, and genetic-physical interaction with DNAAF2, we propose that DYX1C1 represents a novel axonemal dynein assembly factor (DNAAF4).

Online Material and Methods

Whole mount *in situ* hybridization of *Dyx1c1* mouse embryos

Sense and antisense probes for *Dyx1c1* were made from a 554 bp pCRII-TOPO construct (nt 1098 – 1651; RefSeq NM_026314.3, *Mus musculus Dyx1c1* transcript variant 1) made by TOPO TA cloning (Invitrogen) after amplification from complementary DNA. Primers used for amplification were 5´-aaacctacacaaggccatcg-3´ (*Dyx1c1*-F) and 5´-atcctggcaatttcaacagc-3´(*Dyx1c1*-R). Probes were synthesized with digoxigenin NTPs (Roche) after template linearization with Hind III (antisense) or Not I (sense) before RNA synthesis with T7 or SP6 RNA polymerases, respectively. For whole mount in situ hybridization (WISH) staged embryos were fixed overnight at 4°C in 4% paraformaldehyde in 1× PBS. WISH was then performed according to standard procedures with minor modifications[47]. Stained samples were transferred into 80% glycerol, and images were captured using a Scion CFW-1310C color digital camera mounted on an Axioskop2 plus microscope (Zeiss) and Image-Pro Express.

Immunohistochemistry of mouse tissue

Mice were perfused transcardially with 0.9% saline followed by 4% paraformaldehyde (Electron Microscopy Science, Hatfield, PA) in 1× PBS. Brains were removed, fixed overnight in the same fixative at 4°C, and washed in 1× PBS three times for 40 min the next day before cutting into 50 μm sections with a vibratome (VT-1000S; Leica, Wetzlar, Germany). Nuclei were counterstained with Hoechst33342 (2μg/ml PBS, Sigma). Stained sections were washed for 10 min in PBS, coverslipped using prolong gold anti-fade (Invitrogen), and imaged on a Carl Zeiss Axiovert 200M Inverted microscope with an ApoTome attachment and Axiovision 4.6 software (Carl Zeiss). Whole mounts of the entire lateral wall of the lateral ventricles were prepared as described previously[48] and fixed overnight in 4% paraformaldehyde in PBS at 4°C, and washed in 1× PBS three times for 40 min the next day. They were then permeabilized with 0.1% Triton X-100 (Sigma, St. Louis, MO) in PBS for 10 min, blocked in 10% goat serum (Invitrogen, Carlsbad, CA) in PBS/0.1% Triton X-100 for 1 h, and incubated with the following primary antibodies: mouse anti-acetylated tubulin (1:500; Sigma, T6793); rabbit anti-β- catenin (1:100; 9562, Cell Signaling Technology, Beverly, MA) and mouse anti-γ-tubulin (1:500; T6557, Sigma).

After washing three times in PBS, tissues were incubated with appropriate Alexa Fluor dye-conjugated secondary antibodies (Goat anti-rabbit 488 [A11008], Goat anti-mouse 488 [A11001], Goat anti-rabbit 568 [A11011], Goat anti-mouse 568 [A11031] Invitrogen) at a dilution of 1:400 for 1 h. Tissues were washed in PBS and incubated for 5 min in 2 μg/ml Hoechst33342 (Sigma) for counterstaining of nuclei. Secondary antibodies alone were used as a control. Whole mounts were placed onto depressed glass slides and coverslipped with CoverWell imaging chambers (Grace Bio-Labs, Bend, OR). Samples were imaged either on a Carl Zeiss Axiovert 200M Inverted microscope with an ApoTome attachment and Axiovision 4.6 software (Carl Zeiss) or on a Leica TCS SP2 confocal laser-scan microscope.

Immunofluorescence of dissociated mouse nasal epithelial cells

Nasal epithelial cells were harvested from mouse septa by acute dissociation on a 4-well slide in 1:1 PBS/HBSS. The slides were dried to let the cells stick to the wells and then immediately fixed with 4% PFA for 2 min at RT. The cells were then washed with 1× PBS for 2 min each twice. Blocking buffer (10% Goat serum, 0.1% Triton in 1X PBS) was added for 15 mins at RT. The slides were incubate with rabbit polyclonal anti-DYX1C1 antibody (Sigma SAB4200128) at a dilution of 1:500 and mouse monoclonal anti-acetylated tubulin (Sigma, T7451) at 1:1000 in the same blocking buffer for 30 mins at RT. After 3 washes with 1X PBS for 5 min each, the slides were incubated with goat anti-rabbit 488 (Invitrogen, A11034 dilution 1:5000) and goat anti-mouse 568 (invitrogen, A11031 dilution 1: 1000) for 20 min at RT. The slides were washed 2 times with 1X PBS for 5 min each and nuclear stain Hoechst33342 (Invitrogen, H3570) at 1:2500 was added for 15 min at RT. Slides were dried and coverslipped with Prolong Gold antifade (Invitrogen, P36930). The cells were imaged on Leica TCS Sp2 laser scan microscope.

Transmission electron microscopy

For harvesting the brains, mice (12 days old) were perfused transcardially with 0.9% saline followed by 2% paraformaldehyde/2.5% glutaraldehyde in 0.1 mM phosphate buffer (PB). Brain samples were further fixed by immersion overnight in 2% paraformaldehyde/2.5% glutaraldehyde in 0.1 mM PB; and washed in PB three times for 40 min. Sections were postfixed with 2% OsO4 in 0.1 mM PB for 1.5 h and dehydrated through a graded ethanol (EtOH) series. Following dehydration, tissues were twice washed in acetone and embedded in epoxy resin in capped inverted Beem capsules. Thin sections were cut with a diamond knife, placed onto Formvar-coated slot grids, and heavy metal stained with uranyl acetate and lead citrate. Trachea tissues were directly dissected without perfusion and fixed by immersion overnight in 2.5% glutaraldehyde/2% paraformaldehde in 0.12 mM PB. They were washed in PB three times (60 min in total), postfixed in 1% OsO4 and 0.8% potassium ferricyanide in 0.12M PB for 1 hour, dehydrated through graded EtOH series, rinsed twice in acetone and embedded in epoxy resin. Thin sections were cut with diamond knife, placed on copper grids, and heavy metal stained with ethanolic uranyl acetate and Sato's lead citrate. Electron micrographs were captured using an FEI Tecnai 12 Biotwin TEM equipped with a side mounted AMT XR-40 CCD Camera and Epson Expression 1680 flatbed scanners.

Scanning electron microscopy

Wildtype and mutant mice embryos (E7.5 days) were harvested and fixed in 1.5% paraformaldehyde/1.5% glutaraldehyde (Electron Microscopy Science) in 0.10 M sodium cacodylate containing 0.05 M NaCl overnight at 4°C. Samples were postfixed with 2% OsO_4 in the same buffer overnight followed by graded ethanol dehydration. Specimens were dried in a Polaron (Hertfordshire, UK) E3000 Critical Point Dryer and mounted onto aluminum specimen mounts (Ted Pella) using carbon tape and silver paint (Ernest F. Fullam, Clifton Park, NY). Each mount was sputter coated with gold palladium (60% gold, 40% palladium) using a Polaron E5100 Sputter Coater. Samples were examined and photographed using a LEO DSM982 field emission SEM.

Western blots of brain, lung and trachea lysates

Wild-type and mutant animal brains and lungs were harvested and lysed in RIPA Buffer (Sigma) supplemented with 1× Protease Inhibitor Cocktail (Sigma). For tracheal and lung preparation, tissues were dissected and carefully separated from the surrounding tissues. The samples were homogenized using a tissue homogenizer and cleared by centrifugation at 10,000×g for 10 min. Proteins were separated on 10% SDS-PAGE minigels and then transferred to Immobilon (Millipore Inc., Billerica, MA, USA) membrane for Western blotting. For detecting Dyx1c1 protein, the N-terminal DYX1C1 (Sigma, SAB4200128) antibody was used at a dilution of 1:200, anti-Gapdh antibody (Sigma, G8795) was used at 1:1500 as a loading control. Licor Odyssey infrared secondary antibodies were used at a dilution of 1:10,000 (goat anti-mouse 680 [926–32220]; goat anti-mouse 800 [926–32210]; goat anti-mouse 680 [926–32221]; goat anti-mouse 800 [926–32211]) were used at dilution of 1:10,000. All blots were imaged and analysed by Licor Odyssey Scanner and Software.

Immunoprecipitation

Immunoprecipitation assay was performed using Dynabeads Protein G Immunoprecipitation Kit (Invitrogen). Briefly, Dynabeads were resuspended in the vial and separated on a magnet from the solution. N-terminal Dyx1c1 antibody (5μg) was diluted in 200 μL of Washing and Binding Solution and incubated with rotation for 60 min at room temperature. The beads-antibody complexes (beads-Ab) were separated on the magnet, washed by gentle pipetting and separated. Protein lysates as described earlier from the wildtype and mutant mice brains were incubated with the beads-Ab overnight at 4C. The beads-Ab-antigen complex was then washed using the washing solution 3 times. The complex was then incubated with elution buffer for 10–15 mins to dissociate the complex. The beads were separated on a magnet and the supernatant containing the proteins was separated by SDS–PAGE and analysed by western blotting using anti-DNAI2 monoclonal antibody (M01, clone 1C8, Abnova, 1:500), anti-Hsp70 (BD Biosciences, 610607, 1:1000) antibody, anti-Hsp90 (BD Biosciences, 610418, 1:1000) antibody, anti-CCT4 (Aviva Systems Biology, ARP34271_P050, 1:500), anti-CCT3 antibody (Proteintech, 10571-1-AP, 1:500), anti-CCT5 antibody (Proteintech, 11603-1-AP, 1:500), anti-CCT8 antibody (Proteintech, 12263-1-AP, 1:500) and anti-IC74 monoclonal antibody (gift from Dr. Stephen King, 1:750). Rabbit IgG was used as a control.

Videomicroscopy of of ependymal flow and cilia in mice

P6–P10 wildtype and mutant mice were deeply anesthetized with isoflurane and then decapitated. Brains were rapidly removed and immersed in ice-cold oxygenated (95% O2 and 5% CO2) dissection buffer containing (in mM): 83 NaCl, 2.5 KCl, 1 NaH2PO4, 26.2 NaHCO3, 22 glucose, 72 sucrose, 0.5 CaCl2, and 3.3 MgCl2. The lateral wall of the lateral ventricle was dissected using a fine scalpel and forceps and immediately observed in a chamber containing 37°C buffer. For visualization of flow, a small amount of Indian ink was placed on the surface of the lateral wall of the dissected ventricle. Movements of Indian ink were observed and recorded with an IR differential interference microscopy (DIC) (E600FN, Nikon) and a CCD camera (QICAM, QImaging, 120fps). For direct observation of cilia movement, mice brains were harvested as above and coronal slices (400 μm) were cut using a vibratome (VT1200S, Leica). Slices from the third ventricle through the fourth ventricle were visualized using IR differential interference microscopy (DIC) (E600FN, Nikon) and a CCD camera (QICAM, QImaging, 120fps). The images were analysed with ImageJ software (NIH).

RNA probes and whole-mount in situ hybridization of zebrafish embryos

DIG-labelled RNA probes were transcribed from linearized DNA templates and used in RNA *in situ* hybridization by standard methods. Antisense probes included *cardiac myosin light chain* (*cmlc2*; *myl7* – ZFIN)[49], *forkhead 2* (*fkd2*; *foxa3* – ZFIN)[50], *preproinsulin* (*ins*)[51] and *southpaw* (*spaw*)[43].

Microscopy of zebrafish embryos

Images of live zebrafish embryos were taken using the ProgressC14 digital camera (Jenoptik) mounted on a Leica MZFL III microscope. Embryos processed for *in situ* hybridization analysis were mounted in modified GMM[52] [100 ml Canada Balsam (C-1795, Sigma), 10 ml methylsalicylate (M0387-100G, Sigma)], visualized using a Leica DMRA microscope at 10× magnification, and photographed with the ProgressC14 digital camera.

Mutational analysis of PCD patients

Signed and informed consent was obtained from patients fulfilling diagnostic criteria of PCD[53] and family members using protocols approved by the Institutional Ethics Review Board at the University of Muenster and University College London Hospital NHS Trust. Genomic DNA was isolated by standard methods directly from blood samples or from lymphocyte cultures after Epstein-Barr virus transformation. Exome analysis of family UCL200 was performed as part of the UK10K Project, as previously described[15]. Amplification of 10 genomic fragments comprising all 10 exons of *DYX1C1* was performed for each exon and patient in a volume of 50 μl containing 30 ng DNA, 50 pmol of each primer, 2 mM dNTPs, and 1.0 U GoTaq DNA polymerase (Promega Corporation, Wisconsin, USA). PCR amplifications were carried out by means of an initial denaturation step at 94°C for 3 min, and 33 cycles as follows: 94°C for 30 sec, 58–60°C for 30 sec, and 72°C for 70 sec., with a final extension at 72°C for 10 min. PCR-products were verified by agarose gel electrophoresis, purified by PCR product pre-sequencing kit (USB, Ohio, USA) and sequenced bi-directionally using BigDye Terminator v3.1 Cycle Sequencing Kit

(Applied Biosystems, California, USA). Samples were separated and analysed on an Applied Biosystems 3730×l DNA Analyzer. Sequence data were evaluated using the Codoncode software (CodonCode Corporation, Dedham, USA).

Transmission Electron Microscopy of human respiratory cilia

Transmission electron microscopy of human respiratory cilia was performed as previously described[17].

High-Speed Video Microscopy Analysis for Ciliary Beat Assessment in human cilia

Ciliary beat was assessed with the SAVA system[54]. Respiratory epithelial cells were viewed with an Olympus IMT-2 microscope (40 phase contrast objective) equipped with a Redlake ES-310Turbo monochrome high-speed video camera (Redlake, San Diego, CA) set at 125 frames. The ciliary beating pattern was evaluated on slow-motion playbacks.

Immunofluorescence of human respiratory epithelium

Respiratory epithelial cells were obtained by nasal brush biopsy (Engelbrecht Medicine and Laboratory Technology) and suspended in cell culture medium. Samples were spread onto glass slides, air dried and stored at −80 °C until use. Cells were treated with 4% paraformaldehyde, 0.2% Triton-X 100 and 1% skim milk (all percentages are v/v) before incubation with primary (2–3h at room temperature or overnight at 4 °C) and secondary (25 min at room temperature) antibodies. Appropriate controls were performed omitting the primary antibodies. Mouse monoclonal anti-DNAI2 (1:200; H00064446-M01 (clone1C8)) was obtained from Abnova. Mouse monoclonal anti-acetylated tubulin (1:10000; T7451-200UL) and rabbit polyclonal anti-CCDC39 (1:300; HPA035364) were obtained from Sigma. Rabbit polyclonal anti-DNAH5 and anti-DNALI1 antibodies were generated as reported[55,56]. Highly cross-adsorbed secondary antibodies goat anti-mouse Alexa Fluor 488 (1:1000; A11029) goat anti-rabbit Alexa Fluor 546 (1:1000; A11035) were from Molecular Probes (Invitrogen). DNA was stained with Hoechst33342 (1:1000; 14533-100MG, Sigma) or DAPI (1:1000; 32670-25MG-F, Sigma). Immunofluorescence images were taken with a Zeiss Apotome Axiovert 200 and processed with AxioVision 4.8 and Adobe Creative Suite 4.

cDNA Cloning

The following clones were purchased from Origene (Rockville, USA): *DYX1C1* (cat no. SC313387), *DNAAF3/C19orf51* (cat no. SC126165), and *CCDC103* (cat no. RC208345). cDNA clones for *DNAAF2/KTU* and *DNAAF1/LRRC50* were amplified in a two-step (nested) PCR reaction from human bronchial epithelial cell cDNA (ScienCell, cat no. 3214) for Gateway cloning. All PCR products were amplified using KOD polymerase according to manufacturer´s directions, recombined with the pDONR201 Gateway vector via BP Clonase II reaction, and subcloned into Gateway entry vectors for myc and 3×FLAG via LR Clonase reaction.

Preparation of human respiratory cell lysates

Human respiratory cells were obtained either by brushing or cell culture (spheroids)[57]. Cells were incubated in 800–1000 μl NP40 or RIPA lysis buffer containing protease inhibitor cocktail (P8340, Sigma-Aldrich) on ice for 30 min and occasionally vortexed. Lysates were spun at 14,000 rpm at 4°C for 10 min. Supernatants were removed into a new tube (cytoplasmic fraction). Pellets were resuspended and incubated in 100–150 μl modified Reeds High salt extraction buffer[58] (30 mM HEPES pH 7.4, 5 mM MgSO4, 0.1 mM EDTA, 625 mM NaCl, 2 mM DTT, 70 mM β-Mercaptoethanol, 0.1% Triton-X 100) lysis buffer containing protease inhibitor cocktail (P8340, Sigma-Aldrich) on ice for 30–60 min and frequently vortexed. Lysates were spun down at 14,000 rpm at 4°C for 10 min. Supernatants were removed into a new tube (axonemal fraction). Lysates were controlled by silver staining using the ProteoSilver silver staining kit (PROTSIL1-1KT, Sigma-Aldrich) and stored at −20°C or −80°C until use. Using this method we obtained two protein fractions, the first enriched for cytoplasmic proteins (cytoplasmic fraction) and the second enriched for axonemal proteins (axonemal fraction). We confirmed enrichment of cytoplasmic proteins with anti-DNAAF2 antibodies (Fig. 5b) and axonemal proteins with anti-LRRC48 antibodies (Fig. 5b).

Co-immunoprecipititation assays of epitope tagged constructs and Western Blotting

HEK293 cells were transfected with plasmids encoding myc- and FLAG-tagged cDNA constructs using Gene Juice (Novagen) at approximately 0.1 μg DNA per ml of media. Within 24 hrs, cells were collected in 1× PBS and lysed in 1 ml of the following buffer: 50 mM Tris-Cl, pH 8.0, 150 mM NaCl, 1% IGEPAL, 0.5 mM EDTA, and 10% glycerol supplemented with protease (Roche Complete) and phosphatase inhibitors (Cocktails 2 and 3, Sigma Aldrich). Lysates were centrifuged at 16,000 × g for 30 min. at 4°C. Approximately 2 mg of each lysate was precleared with 4 μg of rabbit control IgG antibody for 2 hrs. at 4°C, and then incubated with MagSi/protein A beads (MagnaMedics, Germany) for 1 hr. Lysates were then incubated with 4 μg of rabbit anti-FLAG or anti-myc antibody overnight at 4°C, and then incubated with MagSi/protein A beads for 1 hr. to capture immunoprecipitates. Bead complexes were washed four times in lysis buffer and then resuspended in 1× LDS buffer supplemented with DTT (1/8 lysis volume) and heated for 10 min. at 90°C. Lysates were electrophoresed in NuPAGE 4–12% Bis-Tris gels, transferred to PVDF filters, and subsequently immunoblotted with either anti-myc (A7) or anti-FLAG (M2) mouse monoclonal antibodies. PVDF filters were washed three times in TBS-T (10 minutes each) before blocking in 5% BSA for 2 hours at room temperature. Filters were then washed three times (10 minutes each) before incubation with primary antibody (diluted in TBS-T) overnight at 4°C. Filters were washed three times (10 minutes each) and then incubated with secondary antibody for 1 hour at room temperature. Filters were then washed four times and developed by ECL using Prime Western Blotting Detection Reagent (Amersham). Images were digitally acquired using a FUSION-SL Advance Imager (PeqLab) and modified for contrast using Adobe Photoshop v. CS4. All wash and incubation steps were performed with gentle shaking. The following antibodies were used: Rabbit polyclonal anti-DNAAF2 (1:1000; Atlas Antibodies; HPA004113), rabbit polyclonal anti-LRRC48 (1:500; Atlas Antibodies; HPA036040), rabbit polyclonal anti-DYX1C1 (1:1000; ProteinTech; 14522-1-AP); Rabbit polyclonal anti-myc (1:25; clone A-14, Santa Cruz),

mouse monoclonal anti-myc (1:2000; clone A.7, Abcam), rabbit polyclonal control IgG (1:25; sc-2027, Santa Cruz), rabbit polyclonal anti-FLAG (1:250; clone F7425, Sigma Aldrich), mouse monoclonal anti-FLAG (1:2000; clone M2, Sigma Aldrich), goat anti-mouse HRP antibody (1:5000; NA931V, GE Healthcare) and goat anti-rabbit HRP antibody (1:3000; NA934, GE Healthcare).

Yeast-2-hybrid assay

To analyze the binding capacity between DYX1C1 and DNAAF2, plasmids expressing full-length DYX1C1 fused to a DNA-binding domain (GAL4-BD) and full-length DNAAF2 fused to an activation domain (GAL4-AD) were transformed in yeast strains PJ69-4A and PJ69-4α respectively, and subsequently combined by yeast mating and diploids containing both plasmids were selected on media lacking leucine and tryptophane. Interactions were analyzed by assessment of reporter gene activation via growth on media additionally lacking histidine and adenine to detect *HIS3* and *ADE2* reporter gene activation, α-galactosidase colorimetric plate assays (*MEL1* reporter gene, not shown), and β-galactosidase colorimetric filter lift assays (*LacZ* reporter gene). As a positive control, the binding capacity of the known interactors BD-USH2A_icd and AD-NINL_isoB was assessed, and as a negative control the inability of BD-USH2A_icd to bind to only the GAL4 domain (AD-GAL4). Detailed protocols for evaluation protein-protein interactions are available from the authors upon request.

Supplementary Material

Refer to Web version on PubMed Central for supplementary material.

Acknowledgments

We thank the patients and families for participation in this study, the German patient support group "Kartagener Syndrom und Primaere Ciliaere Dyskinesie e.V." and the US PCD foundation.

This work was funded by the “Deutsche Forschungsgemeinschaft” (DFG Om 6/4), the IZKF Muenster (HO), by the European Community's Seventh Framework Programme FP7/2009, under grant agreement no: 241955, SYSCILIA (RR, HO), BESTCILIA under grant agreement no: 305404 (HO) and by the Netherlands Organization for Scientific research (NWO Vidi-91786396 and Vici-016.130.664) (RR) and by grants from the NIH, R01 HD055655, R01 MH056524; P01 HD057853 (JJL); research grant 5 U54 HL096458-06 (MRK, MWL, JLC, MAZ); NHLBI grant 5 R01HL071798 (MRK, MAZ); NICHD grant 2 R01HD048584 (CES, JVT, SC and RDB); NIH grant U01HL098180 (CWL); AHA fellowship (YL). Newlife Foundation grant 10/11/15 (HMM), Action Medical Research grant RTF1411 (MS). UK10K was funded by the Wellcome Trust (award WT091310). This work was supported partially US NIH grants UL1 TR000083 from the NCATS.

References

1. Fliegauf M, Benzing T, Omran H. When cilia go bad: cilia defects and ciliopathies. Nat. Rev. Mol. Cell. Biol. 2007; 8:880–893. [PubMed: 17955020]
2. Kennedy MP, et al. Congenital heart disease and other heterotaxic defects in a large cohort of patients with primary ciliary dyskinesia. Circulation. 2007; 115:2814–2821. [PubMed: 17515466]
3. Ibañez-Tallon I, et al. Dysfunction of axonemal dynein heavy chain Mdnah5 inhibits ependymal flow and reveals a novel mechanism for hydrocephalus formation. Hum. Mol. Genet. 2004; 13:2133–2141. [PubMed: 15269178]
4. Olbrich H, et al. Mutations in DNAH5 cause primary ciliary dyskinesia and randomization of left-right asymmetry. Nat. Genet. 2002; 30:143–144. [PubMed: 11788826]

5. Pennarun G, et al. Loss-of-function mutations in a human gene related to Chlamydomonas reinhardtii dynein IC78 result in primary ciliary dyskinesia. Am. J. Hum. Genet. 1999; 65:1508–1519. [PubMed: 10577904]
6. Panizzi JR, et al. CCDC103 mutations cause primary ciliary dyskinesia by disrupting assembly of ciliary dynein arms. Nat. Genet. 2012; 44:714–719. [PubMed: 22581229]
7. Loges NT, et al. DNAI2 mutations cause primary ciliary dyskinesia with defects in the outer dynein arm. Am. J. Hum. Genet. 2008; 83:547–558. [PubMed: 18950741]
8. Mazor M, et al. Primary ciliary dyskinesia caused by homozygous mutation in DNAL1, encoding dynein light chain 1. Am. J. Hum. Genet. 2011; 88:599–607. [PubMed: 21496787]
9. Duriez B, et al. A common variant in combination with a nonsense mutation in a member of the thioredoxin family causes primary ciliary dyskinesia. Proc. Natl. Acad. Sci. USA. 2007; 104:3336–3341. [PubMed: 17360648]
10. Bartoloni L, et al. Mutations in the DNAH11 (axonemal heavy chain dynein type 11) gene cause one form of situs inversus totalis and most likely primary ciliary dyskinesia. Proc. Natl. Acad. Sci. USA. 2002; 99:10282–10286. [PubMed: 12142464]
11. Schwabe GC, et al. Primary ciliary dyskinesia associated with normal axoneme ultrastructure is caused by DNAH11 mutations. Hum. Mutat. 2008; 29:289–298. [PubMed: 18022865]
12. Knowles MR, et al. Mutations of DNAH11 in patients with primary ciliary dyskinesia with normal ciliary ultrastructure. Thorax. 2012; 67:433–441. [PubMed: 22184204]
13. Merveille AC, et al. CCDC39 is required for assembly of inner dynein arms and the dynein regulatory complex and for normal ciliary motility in humans and dogs. Nat. Genet. 2011; 43:72–78. [PubMed: 21131972]
14. Becker-Heck A, et al. The coiled-coil domain containing protein CCDC40 is essential for motile cilia function and left-right axis formation. Nat. Genet. 2011; 43:79–84. [PubMed: 21131974]
15. Castleman VH, et al. Mutations in radial spoke head protein genes RSPH9 and RSPH4A cause primary ciliary dyskinesia with central-microtubular-pair abnormalities. Am. J. Hum. Genet. 2009; 84:197–209. [PubMed: 19200523]
16. Ziêtkiewicz E, et al. Mutations in radial spoke head genes and ultrastructural cilia defects in East-European cohort of primary ciliary dyskinesia patients. PLoS ONE. 2012; 7:e33667. [PubMed: 22448264]
17. Olbrich H, et al. Recessive HYDIN mutations cause primary ciliary dyskinesia without randomization of left-right body asymmetry. Am. J. Hum. Genet. 2012; 91:672–684. [PubMed: 23022101]
18. Budny B, et al. A novel X-linked recessive mental retardation syndrome comprising macrocephaly and ciliary dysfunction is allelic to oral-facial-digital type I syndrome. Hum. Genet. 2006; 120:171–178. [PubMed: 16783569]
19. Moore A, et al. RPGR is mutated in patients with a complex X linked phenotype combining primary ciliary dyskinesia and retinitis pigmentosa. J. Med. Genet. 2006; 43:326–333. [PubMed: 16055928]
20. Omran H, et al. Ktu/PF13 is required for cytoplasmic pre-assembly of axonemal dyneins. Nature. 2008; 456:611–616. [PubMed: 19052621]
21. Loges NT, et al. Deletions and point mutations of LRRC50 cause primary ciliary dyskinesia due to dynein arm defects. Am. J. Hum. Genet. 2009; 85:883–889. [PubMed: 19944400]
22. Duquesnoy P, et al. Loss-of-function mutations in the human ortholog of Chlamydomonas reinhardtii ODA7 disrupt dynein arm assembly and cause primary ciliary dyskinesia. Am. J. Hum. Genet. 2009; 85:890–896. [PubMed: 19944405]
23. Mitchison HM, et al. Mutations in axonemal dynein assembly factor DNAAF3 cause primary ciliary dyskinesia. Nat. Genet. 2012; 44:381–389. S1–S2. [PubMed: 22387996]
24. Kott E, et al. Loss-of-function mutations in LRRC6, a gene essential for proper axonemal assembly of inner and outer dynein arms, cause primary ciliary dyskinesia. Am. J. Hum. Genet. 2012; 91:958–964. [PubMed: 23122589]
25. Taipale M, et al. A candidate gene for developmental dyslexia encodes a nuclear tetratricopeptide repeat domain protein dynamically regulated in brain. Proc. Natl. Acad. Sci. USA. 2003; 100:11553–11558. [PubMed: 12954984]

26. Bates TC, et al. Dyslexia and DYX1C1: deficits in reading and spelling associated with a missense mutation. Mol. Psychiatry. 2009; 15:1190–1196. [PubMed: 19901951]
27. Marino C, et al. Association of short-term memory with a variant within DYX1C1 in developmental dyslexia. Genes Brain Behav. 2007; 6:640–646. [PubMed: 17309662]
28. Wigg KG, et al. Support for EKN1 as the susceptibility locus for dyslexia on 15q21. Mol. Psychiatry. 2004; 9:1111–1121. [PubMed: 15249932]
29. Meng H, et al. TDT-association analysis of EKN1 and dyslexia in a Colorado twin cohort. Hum. Genet. 2005; 118:87–90. [PubMed: 16133186]
30. Marino C, et al. A family-based association study does not support DYX1C1 on 15q21.3 as a candidate gene in developmental dyslexia. Eur. J. Hum. Genet. 2005; 13:491–499. [PubMed: 15702132]
31. Scerri TS, et al. Putative functional alleles of DYX1C1 are not associated with dyslexia susceptibility in a large sample of sibling pairs from the. UK. J. Med. Genet. 2004; 41:853–857.
32. Chen Y, et al. A novel role for DYX1C1, a chaperone protein for both Hsp70 and Hsp90, in breast cancer. J. Cancer Res. Clin. Oncol. 2009; 135:1265–1276. [PubMed: 19277710]
33. Hatakeyama S, Matsumoto M, Yada M, Nakayama KI. Interaction of U-box-type ubiquitin-protein ligases (E3s) with molecular chaperones. Genes Cells. 2004; 9:533–548. [PubMed: 15189447]
34. Massinen S, et al. Functional interaction of DYX1C1 with estrogen receptors suggests involvement of hormonal pathways in dyslexia. Hum. Mol. Genet. 2009; 18:2802–2812. [PubMed: 19423554]
35. Wang Y, et al. DYX1C1 functions in neuronal migration in developing neocortex. Neuroscience. 2006; 143:515–522. [PubMed: 16989952]
36. Rosen GD, et al. Disruption of neuronal migration by RNAi of Dyx1c1 results in neocortical and hippocampal malformations. Cereb. Cortex. 2007; 17:2562–2572. [PubMed: 17218481]
37. Hoh RA, et al. Transcriptional program of ciliated epithelial cells reveals new cilium and centrosome components and links to human disease. PLoS One. 2012; 7:e52166. [PubMed: 23300604]
38. Ivliev AE, et al. Exploring the transcriptome of ciliated cells using in silico dissection of human tissues. PLoS One. 2012; 7:e35618. [PubMed: 22558177]
39. Vogel P, et al. Congenital hydrocephalus in genetically engineered mice. Vet. Pathol. 2012; 49:166–181. [PubMed: 21746835]
40. Okada Y, et al. Abnormal nodal flow precedes situs inversus in iv and inv mice. Mol. Cell. 1999; 4:459–468. [PubMed: 10549278]
41. Tan SY, et al. Heterotaxy and complex structural heart defects in a mutant mouse model of primary ciliary dyskinesia. J. Clin. Invest. 2007; 117:3742–3752. [PubMed: 18037990]
42. Chandrasekar G, et al. The Zebrafish Orthologue of the Dyslexia Candidate Gene DYX1C1 Is Essential for Cilia Growth and Function. PLoS One. 2013; 8:e63123. [PubMed: 23650548]
43. Ahmad N, et al. A southpaw joins the roster: the role of the zebrafish nodalrelated gene southpaw in cardiac LR asymmetry. Trends. Cardiovasc. Med. 2004; 14:43–49. [PubMed: 15030788]
44. Plagnol V, et al. A robust model for read count data in exome sequencing experiments and implications for copy number variant calling. Bioinformatics. 2012; 28:2747–2754. [PubMed: 22942019]
45. Tammimies K, et al. Molecular Networks of DYX1C1 Gene Show Connection to Neuronal Migration Genes and Cytoskeletal Proteins. Biol. Psychiatry. 2013; 73:583–590. [PubMed: 23036959]
46. Seixas C, et al. CCTalpha and CCTdelta chaperonin subunits are essential and required for cilia assembly and maintenance in Tetrahymena. PLoS One. 2010; 18:e10704. [PubMed: 20502701]
47. Wilkinson DG, Nieto MA. Detection of messenger RNA by in situ hybridization to tissue sections and whole mounts. Methods Enzymol. 1993; 225:361–373. [PubMed: 8231863]
48. Doetsch F, Alvarez-Buylla A. Network of tangential pathways for neuronal migration in adult mammalian brain. Proc. Natl. Acad. Sci. USA. 1996; 93:14895–14900. [PubMed: 8962152]
49. Yelon D, et al. Restricted expression of cardiac myosin genes reveals regulated aspects of heart tube assembly in zebrafish. Dev. Biol. 1999; 214:23–37. [PubMed: 10491254]

50. Odenthal J, Nüsslein-Volhard C. fork head domain genes in zebrafish. Dev. Genes Evol. 1998; 208:245–258. [PubMed: 9683740]
51. Milewski WM, et al. Conservation of PDX-1 structure, function, and expression in zebrafish. Endocrinology. 1998; 139:1440–1449. [PubMed: 9492081]
52. Struhl G. Anterior and posterior compartments in the proboscis of Drosophila. Dev. Biol. 1981; 84:372–385. [PubMed: 20737876]
53. Zariwala MA, et al. Genetic defects in ciliary structure and function. Annu. Rev. Physiol. 2007; 69:423–450. [PubMed: 17059358]
54. Sisson JH, et al. All-digital image capture and whole-field analysis of ciliary beat frequency. J. Microsc. 2003; 211:103–111. [PubMed: 12887704]
55. Fliegauf M, et al. Mislocalization of DNAH5 and DNAH9 in respiratory cells from patients with primary ciliary dyskinesia. Am. J. Respir. Crit. Care Med. 2005; 15:1343–1349. [PubMed: 15750039]
56. Rashid S, et al. The murine Dnali1 gene encodes a flagellar protein that interacts with the cytoplasmic dynein heavy chain 1. Mol. Reprod. Dev. 2006; 73:784–794. [PubMed: 16496424]
57. Olbrich H, et al. Axonemal localization of the dynein component DNAH5 is not altered in secondary ciliary dyskinesia. Pediatr. Res. 2006; 59:418–422. [PubMed: 16492982]
58. Reed W, et al. Characterization of an axonemal dynein heavy chain expressed early in airway epithelial ciliogenesis. Am. J. Respir. Cell. Mol. Biol. 2000; 23:734–741. [PubMed: 11104725]

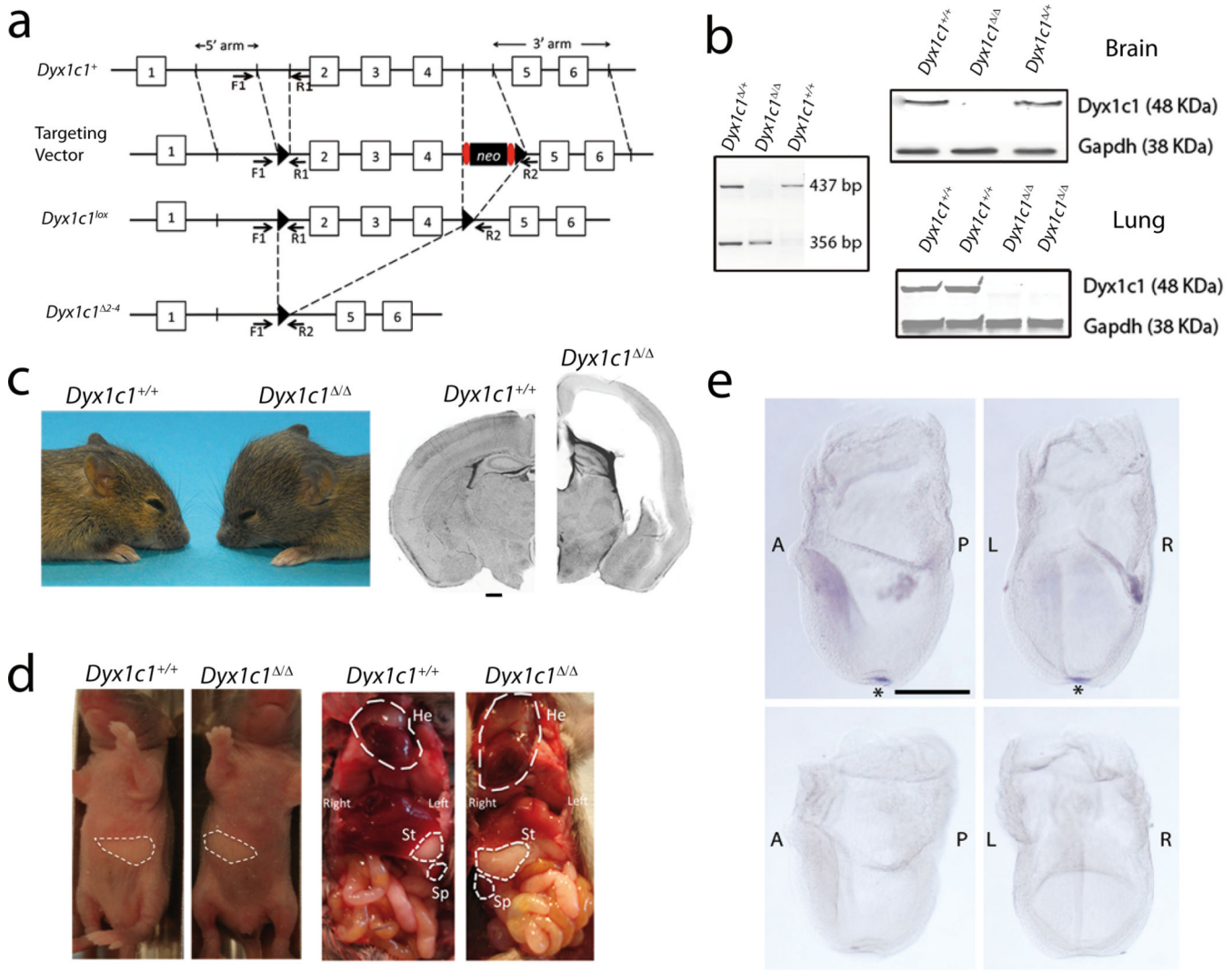

Figure 1. Deficiency of *Dyx1c1* in mouse causes phenotypes consistent with motile cilia defects

(**a**) Schematic of the strategy for producing the *Dyx1c1* exon 2–4 deleted allele. A conditional knockout allele was inserted by homologous recombination and then exons 2–4 were deleted from the germline by breeding mice to an *Hprt-Cre* line of mice. (**b**) Left panel, PCR indicating the genotyping results from the wild-type (F1/R1, 437bp) and deleted alleles (F1/R2, 356bp). Right panels, Western blots show the presence of Dyx1c1 protein detected in brain and lung of wild-type ($Dyx1c1^{+/+}$), and heterozygous animals ($Dyx1c1^{\Delta/+}$), but missing from homozygous mutants ($Dyx1c1^{\Delta/\Delta}$). (**c**) Evidence of hydrocephalus in $Dyx1c1^{\Delta/\Delta}$ mice. Characteristic domed crown in $Dyx1c1^{\Delta/\Delta}$ mice develops by P16 with the ventricles seen in coronal sections are greatly expanded in $Dyx1c1^{\Delta/\Delta}$ relative to $Dyx1c1^{+/+}$ mice. Scale bar, 250mm (**d**) *Situs inversus* in $Dyx1c1^{\Delta/\Delta}$ mice as seen in both the reversal of the milk filled stomach in neonates to the right side, and exposed viscera showing reversal of multiple organs including heart (He), stomach (St), and spleen (Sp). (**e**) Whole mount *in situ* hybridization analysis of *Dyx1c1* in mouse embryos at E7.5. *Dyx1c1* expression is restricted to the pit cells of the ventral node (upper panels: *Dyx1c1* antisense probe, asterisk marks location of node; lower panels: *Dyx1c1* sense control probe; upper and lower left panel: lateral view from the left; upper and lower right panels: frontal view). A, anterior; L, left; P, posterior; R, right; Scale bar, 500μm

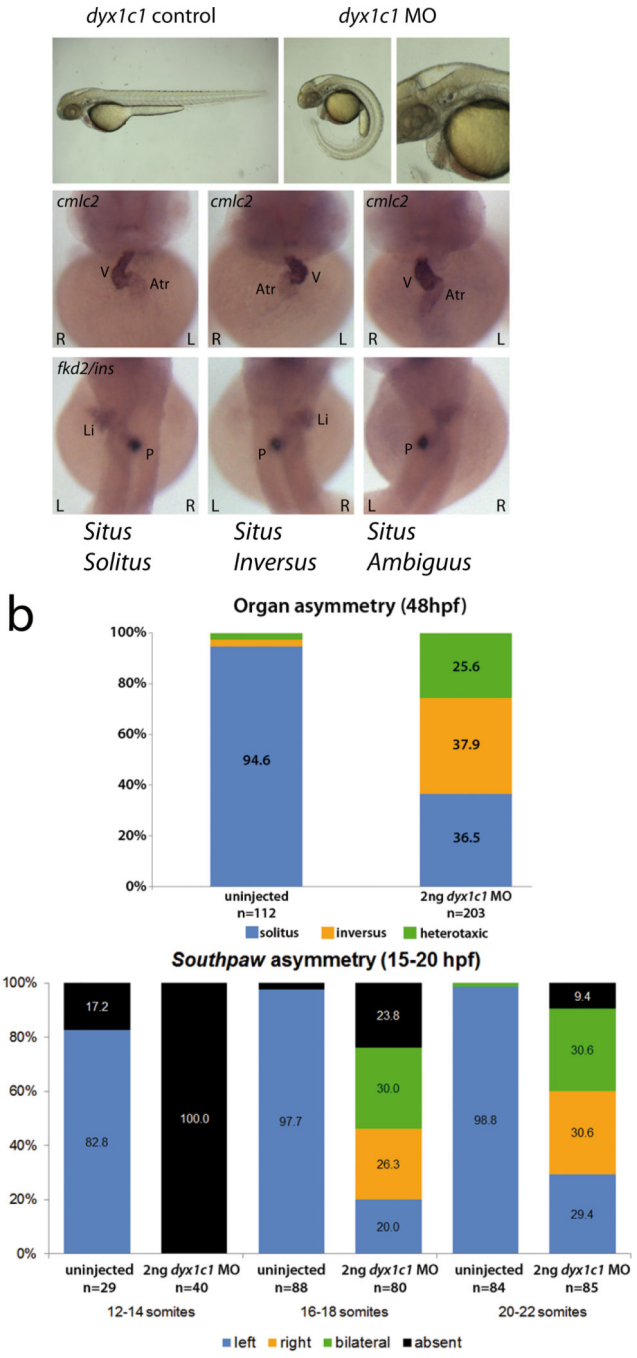

Figure 2. Knock down of *dyx1c1* in *D. rerio*

(**a**) Phenotypes of 48 hpf zebrafish embryos, with AUG-morpholinos (MO) injected between the one- and four-cell stage. Top, lateral images of wild-type and *dyx1c1* morphant zebrafish embryos at 48 hpf. The morphants have a curly tail down phenotype and exhibit hydrocephalus (asterisk in enlarged image) as well as pronephric cysts (arrow in enlarged image). Middle, ventral views of the heart and bottom, dorsal views of the liver and pancreas in *dyx1c1* morphant embryos at 48 hpf. The heart, liver and pancreas were visualized by *in situ* hybridizations for *cmlc2*, *fkd2* and *ins* respectively. L, left; R, right; V, ventricle; Atr, atrium; Li, liver; P, pancreas. Scale bars, 500μm (**b**) Top, graph shows the defects in visceral asymmetry in 48 hpf *dyx1c1* morphant embryos compared to uninjected controls. The laterality defects are associated with 2 ng of *dyx1c1* AUG-MO. Bottom, graph

showing alterations in the asymmetric gene expression of *southpaw* in the LPM of *dyx1c1* morpholino injected embryos compared to uninjected controls at three developmental stages during 15–20 hpf.

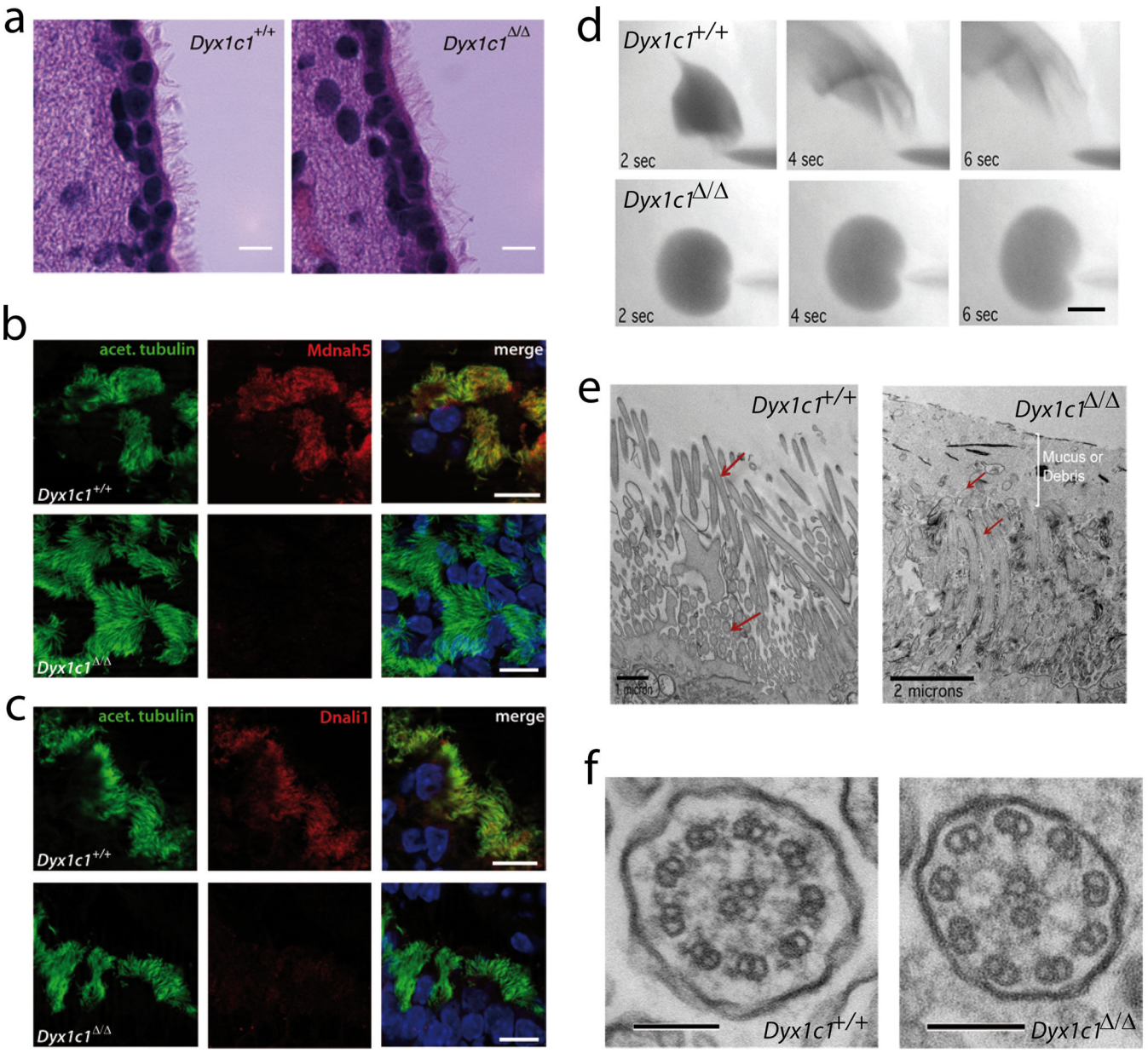

Figure 3. Motile cilia are dysfunctional in *Dyx1c1* mutant mice

(**a**) H&E stained sections of the cerebral ventricles show the presence of cilia on the surface of the ependymal cells in both *Dyx1c1*$^{+/+}$ and *Dyx1c1*$^{\Delta/\Delta}$ mice. (**b,c**) Immunofluorescence analyses of lung sections stained for acetylated tubulin (green), and the outer dynein arm heavy chain Mdnah5 (**b**, red) and inner dynein arm light chain Dnali1 (**c**, red). Nuclei were stained with DAPI. In contrast to *Dyx1c1*$^{+/+}$ mice where Mdnah5 and Dnali1 co-localized with acetylated tubulin (yellow, upper panels in **b** and **c**), in *Dyx1c1*$^{\Delta/\Delta}$ Mdnah5 and Dnali1 (lower panels in **b** and **c**) were completely absent from ciliary axonemes. (**d**) Flow of fluid (Indian ink) across the ependymal surface in brain ventricle cup preparations from a *Dyx1c1*$^{+/+}$ and *Dyx1c1*$^{\Delta/\Delta}$ at mice P6. Directional flow was rapid across the surface of *Dyx1c1*$^{+/+}$ ependymal epithelia, while only non-directional passive diffusion was observed on ependymal surfaces in *Dyx1c1*$^{\Delta/\Delta}$. The starting point for the fluid is at the end of the pipette tip, seen bottom right. (**e**) TEM images of cross-sections through the trachea of wild-type and *Dyx1c1*$^{\Delta/\Delta}$. Abundant cilia were present in each, but cilia structures (red arrows) in the *Dyx1c1*$^{\Delta/\Delta}$ trachea are surrounded by cellular debris and mucus. (**f**) TEM cross section

images of ependymal and tracheal cilia in *Dyx1c1*$^{+/+}$ and *Dyx1c1*$^{\Delta/\Delta}$ mice. The 9+2 microtubular structure was well preserved in *Dyx1c1*$^{\Delta/\Delta}$, except that the outer and inner dynein arms were lacking in tracheal cilia. The scale bars represent in (**a,b,c,d**) 10μm, in (**e**) 1μm (left panel) and 2μm (right panel) and in (**f**) 0.1 μm.

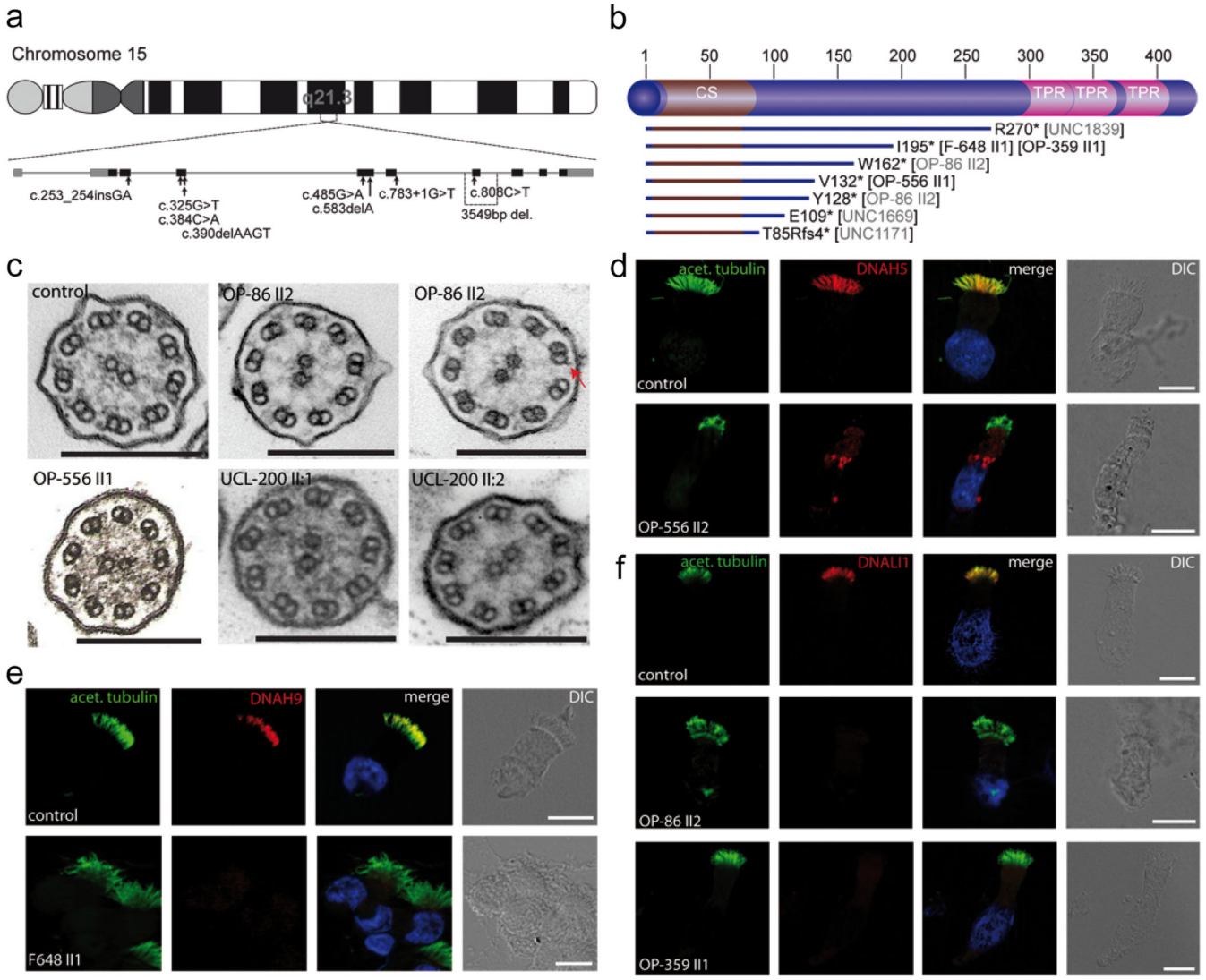

Figure 4. *DYXC1* mutations in human PCD patients cause defective ODA and IDA assembly

(**a**) Schematic presentation of chromosome 15 and the genomic structure of *DYX1C1*. The positions of 8 of the identified mutations are indicated by black arrows, the position of the 3.5kb deletion is indicated by a rectangle. (**b**) Schematic showing the relative positions of seven *DYX1C1* nonsense mutations identified in PCD patients and families in the *DYX1C1* coding sequence. All mutations are clustered in the middle of *DYX1C1* coding sequence and each mutation predicts to cause a premature stop prior to the tetricopeptide repeat domains (TPR) at the C-terminus of DYX1C1 (CS: p23-like C-terminal CHORD-SGT1 domain). (**c**) Transmission electron micrographs showing defects of outer and inner dynein arms in four PCD individuals with *DYX1C1* mutations compared to a control without PCD. Rarely, outer dynein arms can be seen in cilia of the affected patient (OP-86 II2, red arrow). Scale bar, 0.2μm. (**d**) Respiratory epithelial cells from control and PCD patient OP-556 II2 were double-labeled with antibodies directed against acetylated tubulin (green) and DNAH5 (red). Both proteins colocalize (yellow) along the cilia in cells from the unaffected controls. In contrast, in patient cells, DNAH5 was absent from or severely reduced in ciliary axonemes (**Supplementary Fig. 4**). (**e**) Aberrant sublocalization pattern of the outer dynein arm heavy chain DNAH9 in cilia of respiratory epithelial cells from control and PCD patient F648 II1. Cells were double-labeled with antibodies directed against acetylated tubulin (green) and DNAH9 (red). Acetylated tubulin localizes to the entire length of the cilia, whereas DNAH9 localization is restricted to the distal part of the cilia. In contrast, in *DYX1C1* mutant cells DNAH9 was

completely absent from ciliary axonemes. (**f**) Respiratory epithelial cells from control and PCD patient OP-86 II2 and OP-359 II1 were double-labeled with antibodies directed against acetylated tubulin (green) and DNALI1 (red). Both proteins colocalize (yellow) to the ciliary axonemes in cells from an unaffected control, while DNALI1 was absent from the ciliary axonemes in *DYX1C1* mutant cells. In **d, e,** and **f** nuclei are stained with Hoechst33342 (blue). Scale bar, 10μm.

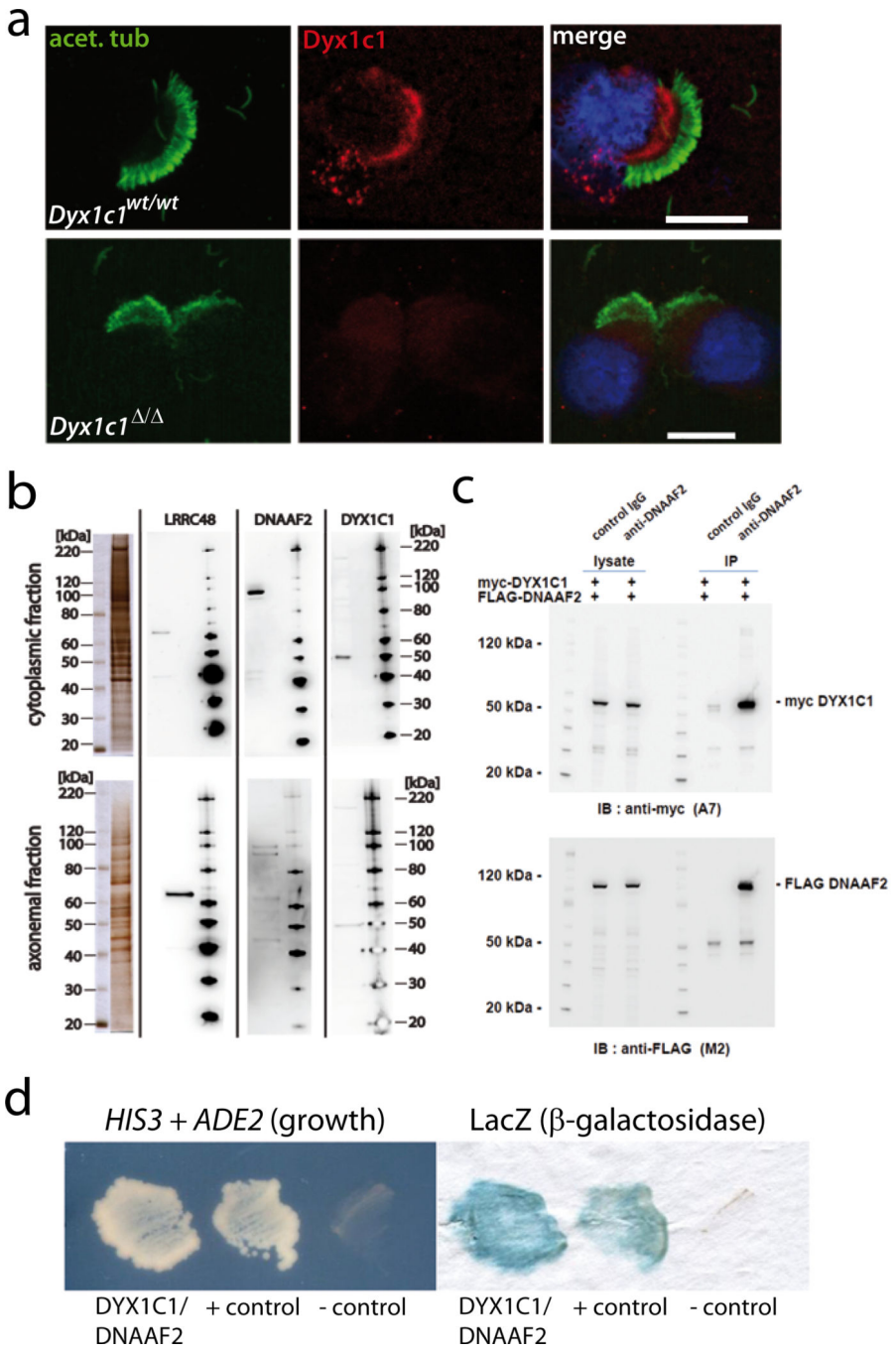

Figure 5. DYX1C1 is localized in the cytoplasm of respiratory epithelial cells and interacts with DNAAF2/KTU

(**a**) Immunofluorescence analyses of mouse nasal epithelial cells stained for acetylated tubulin (green) and Dyx1c1 (red)m. In *Dyx1c1*$^{+/+}$ mice, Dyx1c1 localizes to the cytoplasm of the epithelial cells and partly to the basal bodies but is absent in the cilia. In the mutant, Dyx1c1 is absent from the cytoplasma. Nuclei were stained with Hoechst 33342 (blue). (**b**) Immunoblots performed with different lysate fractions (**a**, cytoplasmic and axonemal) demonstrate that DYX1C1 (right panels), as well as DNAAF2 (middle right panels), shows a strong signal in the cytoplasmic fraction but is almost absent in the axonemal fraction. LRRC48/DRC3 (middle left panels) was used as an axonemal control. Silver staining of the loaded lysates is shown on the left panels. (**c**) HEK293 lysates coexpressing myc-DYX1C1 and FLAG-DNAAF2 were immunoprecipitated with either rabbit

control IgG or rabbit anti-DNAAF2 antibody. Western blotting with mouse anti-myc demonstrates that myc-DYX1C1 is efficiently immunoprecipitated by DNAAF2 (top panel), and Western blotting with mouse anti-FLAG confirms that FLAG-DNAAF2 is recovered in the immunoprecipitate (bottom panel) as compared to the control immunoprecipitation. Equal volumes (12 μl) of lysate and immunoprecipitate fractions were loaded on the same gel; lysate fractions represent 0.7 % of total lysate (1 ml volume) and immunoprecipitate fractions represent 1/15 lysis volume (33 μl resuspension). Magic Mark protein ladder (M) was used to estimate molecular weight of myc-DYX1C1 and FLAG-DNAAF2. The observed molecular weights of myc-DYX1C1 and FLAG-DNAAF2 are higher than the expected molecular weights of 48.5 and 91 kDa due to additional sequence from myc and FLAG epitope tags, respectively. (**d**) Yeast two-hybrid assay using BD-tagged DYX1C1 and AD-tagged DNAAF2 demonstrates a binary interaction between DYX1C1 and DNAAF2. Binary interactions were identified by yeast growth on media lacking adenine and histidine to select for *HIS3* and *ADE2* reporter gene activation (left panel). Interactions were additionally validated by evaluation of *LacZ* reporter gene activation (β-galactosidase colorimetric filter lift assay, right panel). Binding of BD-DYX1C1 and AD-DNAAF2 was validated by using the known interactors BD-USH2A_icd and AD-NINL_isoB as a positive control, and BD-USH2A_icd and AD-GAL4 as a negative control.